Experimental characterisation of cork agglomerate core sandwich panels for wall assemblies in buildings

Ricardo Ferreira *, Diogo Pereira, António Gago, Jorge Proença

CERIS, Instituto Superior Técnico, Universidade de Lisboa, Av. Rovisco Pais 1, 1049-001 Lisboa, Portugal

A B S T R A C T

In recent times, the construction market has seen a very significant increase in the demand of pre-fabricated solutions of nonstructural elements, such as sandwich panels for buildings walls. Due to the inherent low weight, good mechanical behaviour, ease of assembly and cost-effectiveness, these types of wall assemblies are especially competitive in construction of single-family houses or one unit dwelling structures.

However, the low fire resistance of many of these solutions, such as sandwich panels with expanded polystyrene core or polyethylene terephthalate foam core, precludes their use in buildings with more than one floor. The substandard fire resistance is generally due to the fact that the constituent materials are combustible or, at least, their properties are extremely sensible when subjected to high temperatures or flame.

Given the isolation properties, good mechanical damping and fire resistance, cork agglomerate can be used as the core material for sandwich panels. However, this material is heavier than the other materials commonly used as core for sandwich panels. In order to deal with this drawback, it is necessary to choose a material for the panel facings that could fulfil the mechanical requirements and the condition not excessively increase the panel weight. The use of a glass fibre reinforced polymer seemed a suitable solution for the facing component. Therefore, the proposed wall assembly solution consists in a sandwich panel with cork agglomerate core and glass fibre reinforced polymer facings.

The scope of this work was the assessment of the feasibility of a new configuration of vertical (wall) sandwich panels that could, not only be a cost effective solution for prefabricated construction, but also provide good mechanical performance and fire resistance. This sandwich wall panel configuration was tested for characterisation of its mechanical behaviour, resistance to impact and to fire. The results of the experimental campaign carried out are presented in this manuscript along with some conclusions about the suitability of this solution as sandwich wall panel for buildings façades.

© 2016 Elsevier Ltd. All rights reserved.

1. Introduction

The use of composite materials has seen a significant increase over the last few decades, especially in the transport and aerospace industries, mainly due to the search for structures that are both lighter and. In the last ten years, the construction industry has been no stranger to such development, particularly in developing repair and strengthening solutions for old structures and composite structures for partition and external walls.

In some cases, the traditional brick construction for partition and external non-structural walls in buildings has successfully been replaced by updated pre-fabricated composite wall solutions such as sandwich wall panels, especially in situations where low weight is needed. In the context of building construction, sandwich wall panels of polyurethane or expanded polystyrene cores and glass fibre reinforced polymer facings are the most popular solutions [1–4]. Among the advantages of these wall panels are their low weight, adaptability to uncommon shapes (e.g., non-orthogonal or non-rectangular), and their thermal and acoustic properties. In recent years, several materials and configurations have been studied for potential use for sandwich panel.

However, the poor fire resistance of the materials widely used in sandwich panels, such as resins, polystyrene and polyurethane, precludes their use in many situations. Furthermore, sustainable development requisites and ecological concerns regarding energy consumption have to be taken into consideration.

Extensive studies have also been carried out to assess the fire resistance of composite panels [5–9] and [10]. It is therefore desirable to address this problem by using ecological, sustainable, core materials with high fire resistance and that do not unduly

sacrifice the mechanical requisites for walls. Given these premises, this research aims to evaluate the potential use of cork agglomerate as core material for sandwich panels to be used as partition or external walls.

Cork is the natural bark produced by the cork oak (*Quercus suber* L.). It is a natural lightweight material that has interesting properties, including elasticity, low permeability to gases and liquids, good thermal insulation and high damping capacity and durability [11].

According to [11], cork has an alveolar cellular structure similar to that of a honeycomb and its cells are mostly formed by suberin, lignin and cellulose. This composition has a strong influence on the mechanical properties of cork-based materials

Cork agglomerates (CA) are produced from cork waste and residues through an industrial process. This waste (in granules) is autoclaved at high temperature and pressure without the use of an additional adhesive. This industrial process induces the thermochemical degradation of the cork cell wall, through prior expansion of the granules.

The temperature and pressure applied cause all the granules to be covered by suberin and waxes that can diffuse and deposit on the cork granule surfaces. The result is a corkboard that can be used for multiple purposes. CA retains some of the advantages provided by natural cork such as good thermal insulation, low water and acoustic absorption, good vibration damping and chemical resistance. In addition, CA is an economically and environmentally sustainable material.

The paper describes the experimental work involved in the creation and physical validation of a CA core sandwich panel. It is part of a research project aiming to develop an innovative building construction system. In addition to the potential mechanical and fire behaviour benefits, this solution offers ecological and sustainability benefits [12]. This study focused on the mechanical and impact behaviour, as well as the fire resistance of sandwich panels with CA core. The assessment was conducted bearing in mind the recommendations of the relevant ISO and ASTM.

2. Previous studies and experimental investigation

A wide variety of materials and configurations have been developed and tested for potential use in sandwich panels, particularly in the transport and aerospace industry. Some relevant experimental studies conducted on sandwich panels for building construction and other purposes are briefly summarised next.

Smakosz and Tejchman [13] carried out a series of experiments to analyse the strength, deformability and failure mode of panels made from expanded polystyrene (EPS) foam core and glass–fibre facings reinforced with magnesium-cement. The aim was to describe the mechanical behaviour of such panels and their components under bending, compressive and tensile quasi-static monotonic loads. For this purpose, large- and small-scale specimens were tested. Impact and thermal behaviour were also addressed through experimental testing. Tests showed that the general behaviour of these panels under loading is initially linear, then slightly non-linear and finally brittle at failure. In the bending tests, failure was due to tensile failure of the bottom facing, whereas in compression failure was due to crushing of the facings (without local or overall buckling of the facing).

As for the impact behaviour of these panels, tests showed insignificant penetration and traces of damage on the panel surface and thus both the serviceability and safety requirements of panels against impacts were satisfied. Finally, the thermal results showed that the effect of the gradient temperature on the panel deformation was negligible.

Zinno et al. [1], reported the experimental characterisation of a different kind of panel that used an alternative material for the sandwich panel core. A phenolic-impregnated honeycomb core produced with Nomex (aramid paper/phenolic resin) was chosen. The scope of this study was to determine the efficiency of this material in terms of its structural and impact behaviour, with a view to using it in the transport industry. The same authors also assessed the environmental degradation of the component materials through accelerated ageing tests. The sandwich experiments involved both compressive and bending quasi-static tests to evaluate the compressive and shear mechanical properties of the core and to shed light on the bending behaviour effects in the stiffness and failure modes.

Average values estimated for the mechanical properties such as compressive modulus E, compressive strength σ and shear modulus G were derived from the quasi-static experimental tests. The structural performance of phenolic-based core sandwich structures subjected to environmental effects was also assessed experimentally by means of accelerated ageing. Finally, the experimental work also included ballistic impact tests to understand the response of the sandwich material and the damage mechanisms involved when a sandwich structure suffers an impact. The dynamic impact tests showed that the facings are mostly responsible for the overall behaviour and energy absorption.

Castro et al. [14], carried out an investigation to optimise the mechanical properties of cork-based agglomerates intended to be used as sandwich panel components for lightweight structures. Consequently, three new types of cork agglomerate consisting of cork granules and epoxy resin were produced and tested.

The experiments carried out by Castro et al. comprised three different types of behaviour characterisation tests: mechanical tests, impact tests and thermal conductivity tests. The tested sandwich panels consisted of carbon/epoxy facings and several different core materials, namely, Nomex, Rohacell 71 WF rigid foam, commercial cork agglomerates (of 3 different densities) and enhanced cork agglomerates. The enhanced cork agglomerates consisted of conventional cork agglomerate with epoxy resin added to the adhesion process of the cork granules.

Regarding the cork agglomerates' mechanical behaviour, test results showed that their performance essentially depends on the cork granule size, its density and the bonding procedure used for the granulates. The authors also concluded that the aforementioned parameters can be adjusted according to the final application intended for the sandwich panel.

The highest maximum core shear stress was recorded for the Nomex core sandwich specimens, followed by the cork-epoxy agglomerate cores (1–12% lower than Nomex, 38–56% higher than Rohacell rigid foam and four to seven times higher than the commercial cork agglomerates). Maximum stress at the facing and panel shear rigidity values were also found in Nomex/carbon and Rohacell/carbon sandwiches. Values of those stresses in the cork-epoxy core sandwich specimens were nearly three times higher than in the conventional cork agglomerates.

Concerning the impact test results, the authors concluded that the impact performance of cork-epoxy and conventional cork agglomerates had a similar behaviour, but slightly higher impact forces were obtained for cork-epoxy composites. The authors observed that cork agglomerates are characterised by their rapid response to transient loads, which, together with the elastic behaviour demonstrated in the bending tests, could be considered as a minimising factor with respect to the probability of extensive damage. The authors also reported the excellent recovery capacity exhibited by the cork-based sandwich panels' displacement curves, regardless of the type of cork agglomerate and fabrication method.

Finally, regarding the thermal behaviour tests, the authors concluded that cork agglomerates with lower densities had better

thermal properties, which is important when considering the design of mechanically efficient structures with low weight requirements (such as aerospace components).

Hoto et al. [15] carried out experimental investigations concerning the bending and water absorption behaviour of a composite asymmetric sandwich using cork core agglomerates.

In this study [15], cork agglomerate and natural fibre facings, particularly basalt and flax fibre, were used to manufacture the sandwich specimens. The authors used two different types of cork agglomerates: current cork agglomerate and an epoxy resin-impregnated cork agglomerate.

For the mechanical behaviour tests, since the sandwich specimens were asymmetric, each type of specimen was tested in two different arrangements (Basalt Up or Flax Up).

In [15] authors observed that the kind of failure mechanism was strongly influenced by the test configuration as well as the core type. For specimens with modified cork agglomerate core, with basalt layers as upper facing, the sandwiches underwent a sequence of three failure mechanisms: the initial failure began at the lower facing; the crack then grew through the core, and finally delamination occurred between the core and upper facing. An abrupt load drop caused by the failure of the bottom facing shows the poor load bearing capacity of flax under a tensile load. The authors stated that this behaviour could be associated with the fact that the modified cork agglomerate core, being more rigid, is more prone to crack growth. In case of specimens with current cork agglomerate core, as the core was not stiff enough to withstand the stress the upper facing showed shear failure and no significant damage appeared at the bottom facing. When flax fibre layers were used for the facing, the specimens' failure sequence was by initial compressive failure followed by core densification. After reaching peak load, only slight load loss could be observed and the specimens then continued to carry a significant load. No significant failure was observed in the lower basalt facing. The average load on the horizontal plateau of the load–displacement curve remained significant. Inspection of the sandwich after failure showed matrix cracking and facing wrinkling at the load application point. The authors stated that the modified cork panel offers better resistance to deformation under compressive load because of the resin surrounding the cork granules, which deflects the stresses along the interfaces and thus delays the compressive deformation.

Davies et al. [5], published an extended state of the art report on the numerical modelling of the performance of polymer composite structural members and components at high temperature. First, the authors reviewed the methods available for thermal modelling and then they reviewed the thermo-mechanical modelling. Afterwards, numerical and experimental analyses were performed to assess the mechanical properties of polymer composites at high temperatures.

In [5], the experimental work also included the thermo-mechanical analysis of sandwich composites with phenolic foam cores. The authors found that the phenolic foam core did not perform satisfactorily. However, they claim that with higher density phenolic foam cores the composites should have improved fire performance.

Mouritz and Gibson [10] have also addressed fire behaviour and its interaction with materials. They gathered a significant amount of information on the main aspects of the fire performance of polymers, in particular on the thermal decomposition of polymers in fire, fire reaction of composites, fire damage to composites, fire resistance of polymers and fire retardants.

In [10] the authors first addressed the subject of fire behaviour of polymers by showing how examples of fire outcomes in several scenarios illustrate the importance of understanding the fire properties of composites and the need to use flame retardant polymers in all composite materials. According to [10], and in spite of their outstanding fire performance, cost still is the major deterrent to using flame retardant composites. However, the authors do not address the fire behaviour of other composites such as natural fibre composites, claiming that the flammability of these materials is not a serious concern.

The authors say that some polymer composite materials are not recommended to be subjected directly to fire because of the poor behaviour of some of their components. Under high temperatures, these components release highly flammable hydrocarbon gases that act as additional fuel for the combustion process.

According to [10], another relevant factor in the decomposition of polymers is its thermal diffusion. This is particularly important when polymers are used in partition walls and one facing is subjected to fire. Thermal diffusion of the materials used will affect the heating rate between the exposed and the unexposed facings and will therefore affect the decomposition reactions throughout the depth of those partition walls.

The same authors [10] found that fire damage to sandwich composites with combustible facings and core shows a similar pattern: first, there is char formation on the skin of the face subjected to the heat flux, then the resin softens and deteriorates, and finally delamination and matrix cracking occur. Core deterioration starts to occur once the face skin becomes severely damaged and is unable to provide significant thermal protection. As the core material decomposes with increasing fire exposure, it detaches from the charred facing and the decomposition and char zones of the core tend to move towards the unexposed facing. Finally the authors noted that for sandwich composites with Nomex paper, honeycomb and polyurethane foam cores suffered severe decomposition and volatilisation, leaving little residual char between the facings.

3. Materials and generic testing setups

The wall panel system under development is a three-layered sandwich panel composed of two 1 mm thick GFRP facings and one 80 mm thick CA core. The GFRP facings are made of resin impregnated glass fibre textile with a nominal specific weight of 7.5 N/m^2. Bonding between the CA core and the GFRP facings is obtained with an epoxy adhesive. The epoxy resin has density 11 kN/m^3 and viscosity 0.70–1.10 Pa s at a temperature of 25 °C, and the hardener has density 9. 5–10.8 kN/m^3 and viscosity 0.10–0.15 Pa s at a temperature of 25 °C.

The cork agglomerate used has density 1–1.25 kN/m^3, thermal expansion coefficient 40×10^{-6} °C^{-1}, tensile strength of 50–80 kN/m^2 and compressive strength at 10% strain of 150–180 kN/m^2.

All mechanical tests were carried out in LERM (Structures and Strength of Materials Laboratory of Instituto Superior Técnico-IST, U Lisboa), using INSTRON 1343, a uniaxial test machine [16]. The INSTRON 1343 has hydraulic crosshead lifts, clamping devices, wide stance feet and internal transducers (force and stroke). This equipment was designed to perform a wide range of dynamic (including fatigue) and static tests on materials and structural component specimens within the following ranges: ± 50 mm (stroke) and ± 250 kN (range).

The data acquisition unit digitised and stored the outputs for the load (F) and the related displacement (δ, stroke) provided by the INSTRON 1343 internal transducers (Fig. 1).

The impact tests were performed using a test steel frame to enclose and fix the test specimens, their connections (the top and bottom connections of the specimens replicate the connection detailing of the relevant construction system) and the pendulum system used for impact simulation.

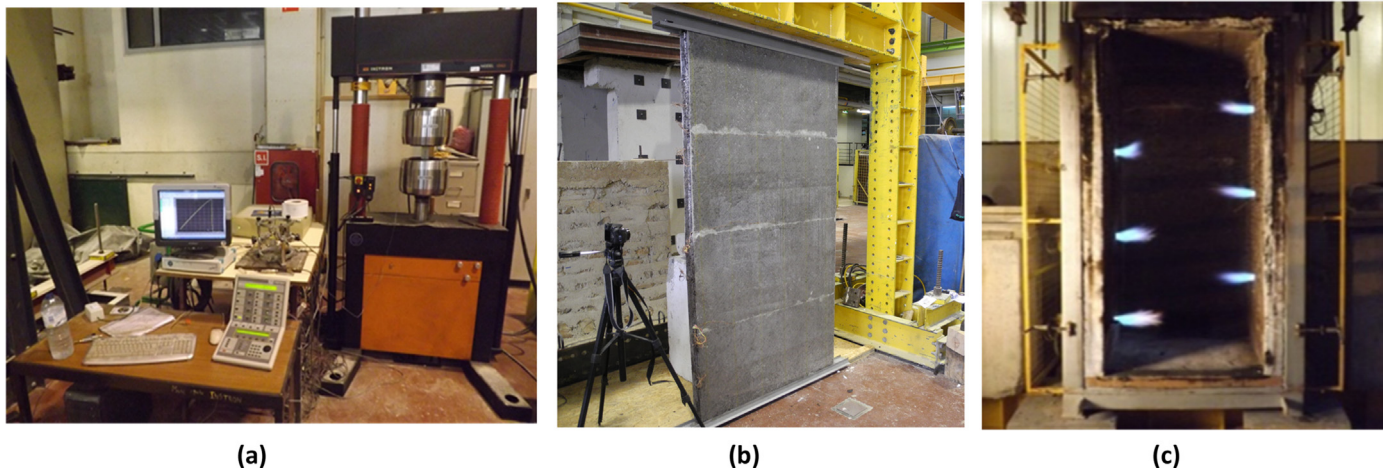The impact tests were performed using full-scale sandwich

Fig. 1. Test apparatus used for testing: (a) INSTRON 1343 and the data recording equipment; (b) setup for impact tests on the panels and (c) LERM vertical furnace for fire resistance tests.

wall panels together with their top and bottom connection systems, thus replicating as realistically as possible the actual support conditions for wall panel assembly in buildings. The setup for these tests consisted of the steel frame to secure the test specimens and a pulley and cabling system to lift and release the impact bodies. The energy imparted in each test, E_i, was controlled by combining different masses, M_i, of the impact bodies and release heights, H_i. More details about the test are presented later.

The fire tests used a vertical furnace through which the panels were subjected to a standard time–temperature curve. The furnace was fired by internal gas burners and the heat was controlled by measuring the temperature through thermocouples located inside the furnace. The gas feed was automatically controlled so that the inside temperature evolution closely matched the standard time–temperature curve defined in EN1363-1 [17]. In each test, the panel covered the front opening of the furnace to fully expose the inner facing to the heat.

4. Mechanical tests

The following mechanical tests were performed in accordance with the specified standards:

- Flatwise compressive properties of cork agglomerate core CA (ASTM 365) [18].
- Edgewise compressive strength of CA core and GFRP facings (ASTM 364) [19].

- Beam flexure test of composite specimens composed of CA core and GFRP facings (ASTM C393/C393 M, [20]; ASTM D7249/D7249M, [21] and ASTM D7250/D7250M, [22]).
- Impact tests on panels composed of CA core and GFRP facings (ISO 7892) [23].

Additionally, fire resistance tests were performed in accordance with the fire classification of construction products and building elements (EN 13501-2) [17].

The statistical treatment of all the results obtained in testing used the average ($\bar{X}$), standard deviation (S_{n-1}) and variation coefficient (CV) values.

4.1. Flatwise compressive properties of the cork agglomerate core

The objective of these tests was to measure the flatwise compressive strength (σ_{cn}^{ult}) of the CA core and the corresponding compressive modulus (E_{cn}). The tests and computations carried out followed [18] for the experimental determination of the compressive strength and modulus of sandwich cores.

Ten test specimens (FC1–FC10) were used for these flatwise compressive tests. The first set of five specimens (FC1 to FC5) had GFRP facings and the other five specimens had no facing of any kind (FC6–FC10). This differentiation was introduced to analyse the influence of the GFRP facings on the specimens' flatwise compressive properties (σ_{cn}^{ult}) and (E_{cn}). A uniformly distributed load over the specimens was achieved by fitting the universal testing machine with thick steel plates clamped to the crosshead

Fig. 2. Unloaded specimen (a) and fully loaded specimen (b).

Table 1
Results of the flatwise-compressive tests (a) with GFRP facings and (b) without GFRP facings.

	Test specimens	F_{max} (kN)	δ (mm)	σ_{cn}^{ult} (kPa)	E_{cn} (MPa)		Test specimens	F_{max} (kN)	δ (mm)	σ_{cn}^{ult} (kPa)	E_{cn} (MPa)
With GFRP facing	**FC1**	0.62	1.66	61.48	3.07	**Without GFRP facing**	**FC6**	0.65	1.61	65.54	3.28
	FC2	0.66	1.66	65.59	3.28		**FC7**	0.64	1.62	63.72	3.19
	FC3	0.54	1.65	53.92	2.70		**FC8**	0.61	1.61	60.69	3.03
	FC4	0.64	1.66	63.38	3.17		**FC9**	0.62	1.61	61.42	3.07
	FC5	0.63	1.66	62.99	3.15		**FC10**	0.53	1.61	53.04	2.65
	Average ($\bar{X}$)	–	**1.66**	**61.47**	**3.07**		**Average ($\bar{X}$)**	–	**1.61**	**60.88**	**3.04**
	Standard deviation (S_{n-1})	–	0.00	4.47	0.22		**Standard deviation (S_{n-1})**	–	0.00	4.79	0.24
	Variation coefficient (CV)	–	0.23 %	7.27 %	7.27 %		**Variation coefficient (CV)**	–	0.21 %	7.86 %	7.86 %

lift cylinders. Fig. 2 shows the setup used for these tests.

All the tested specimens had the same geometrical shape ($100 \times 100 \times 80$ mm³,; and the facings of specimens FC1 to FC5 were 1 mm thick.

For all tested specimens, failure mode occurred by crushing of the CA core. According to [18], the flatwise compressive strength (σ_{cn}^{ult}) is given by:

$$\sigma_{cn}^{ult} = \frac{F_{max}}{A} \tag{1}$$

According to [18], for cores that do not present a definite maximum value of applied force (F), the values (F_{max}) correspond to the maximum strain (ε) in compression of 2.0%. Table 1 shows the results for (F_{max}) and its corresponding displacement (δ), leading to the computation of the flatwise compressive modulus, given by:
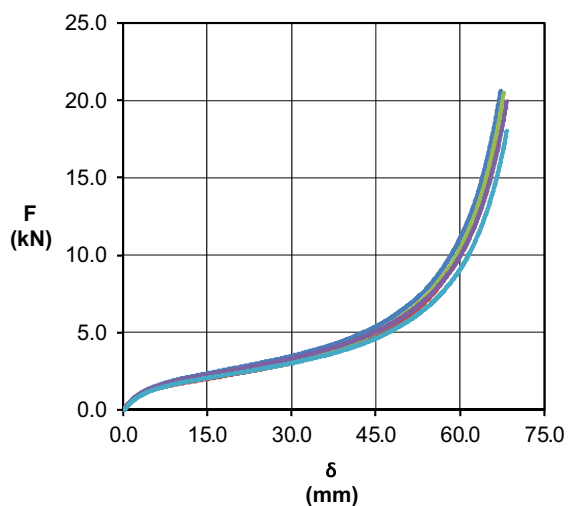
$$E_{cn} = \frac{\Delta F / \Delta \delta \bullet t}{A} \tag{2}$$

where

1. E_{cn} – is the flatwise compressive modulus [MPa].
2. ΔF – is the initial (elastic) load variation [N].
3. $\Delta \delta$ – is the displacement variation for ΔF [mm].
4. t– is the core thickness [mm].
5. A – is the loading area [mm²].
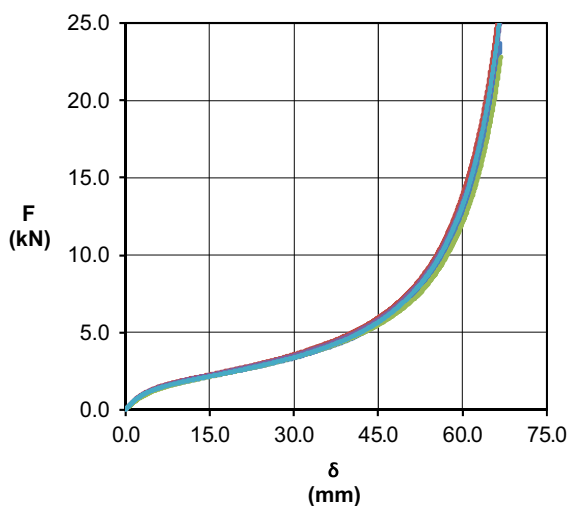
Table 1 shows the computed results for σ_{cn}^{ult} and E_{cn} of test specimens FC1 to FC10.

The results presented in Table 1 show little variation in compression properties with only a small difference between the results obtained for specimens with and without GFRP facing. Average values σ_{cn} (for 2% strain) obtained for specimens with and without GFRP facings were, respectively, 61.47 kPa and 60.88 kPa. Regardless of the existence of GFRP facings, the force–displacement relation (Fig. 3) shows the typical compressive behaviour similar to that of natural cork, as reported in [11,14,15].

These force–displacement curves (Fig. 3) successively exhibit three main regions: (i) linear elastic (between 0% and 2% strain); (ii) similar to a sloping plastic plateau (between approximately 2% and 60% strain); (iii) finally, beyond the 60% strain, with increasing stiffness (possibly because of core densification) until collapse. It was interesting to note the difference in the compressive modulus E in each of these regions. After the first elastic behaviour, a decrease in E of approximately 70% was observed relative to the value obtained for the first region (from approximately 3 MPa to 0.8 MPa), while in the third region (beyond 60% strain), E increased significantly from approximately 0.8 MPa to 6 MPa, almost double the E_{cn} obtained for the first elastic region. The results in Table 1 indicate that the difference between the computed average values for the compressive strength of specimens with and without GRFP facings is negligible (the value of σ_{cn}^{ult} for specimens with GFRP facings is merely 0.96% higher than that of the σ_{cn}^{ult} of specimens without them). The same is observed for E_{cn}, where for

Fig. 3. Results for flatwise compressive tests: (a) results for FC1 to FC2 specimens, and (b) results for FC6 to FC10.

Fig. 4. Setup for the edgewise test.

specimens with GFRP facings E_{cn} is 1% higher than the E_{cn} of specimens without them). This indicates that the compressive behaviour of the composite CA panel will be predominantly governed by the CA's compressive behaviour.

In terms of compressive behaviour, it was interesting to draw a comparison with other tested materials such as EPS and Nomex honeycomb cores.

Tests carried out by [13] on EPS with 0.2 kN/m³ density cores yielded an average compressive strength σ for an EPS core of 110 kPa and an average compression modulus E of 6.09 MPa. Meanwhile, compressive testing of Nomex honeycomb cores with 0.48 kN/m³ density [24] gave an average compressive strength σ of 2.38 MPa and a compressive modulus E of 136 MPa.

The computed values for σ_{cn}^{ult} and E_{cn} of CA (σ_{cn}^{ult}=61.47 kPa, E_{cn}=3.07 MPa) show that despite being five times denser than EPS and 3 times denser than Nomex, the compressive strength of CA core is relatively low (only 50% of EPS compressive strength and only 2.6% of Nomex compressive strength). Additionally, given the presented values for compressive modulus E_{cn} and despite being less dense than CA, EPS and Nomex, the honeycomb cores have higher values of E_{cn}. These rather poor results for the compressive behaviour of CA could be justified by the compressive behaviour of the main components of the CA's inner structure, which are air and cork granules.

4.2. Edgewise compressive strength of the cork agglomerate with GFRP facings

The objective of the edgewise compressive tests (Fig. 4) was to obtain the edgewise compressive strength (σ_s^{ult}) and the corresponding compressive modulus (E_{ct}) of panels with CA core and GFRP facings. Furthermore, this study aimed to assess the contribution of each component, the facings and core, to the compressive strength (σ_s^{ult}) and the compressive Young's modulus (E_{ct}).

The tests and computations were performed following [19]. Ten specimens (EC1–EC10) were used in the edgewise compressive tests. The first five specimens (EC1 to EC5) had GFRP facings and the other five (EC6–EC10) did not have any kind of facing. This distinction was meant to analyse the influence of the (GFRP) facings on the specimen's edgewise compressive properties (σ_{cu}^{lt}) and (A_{ct}). All ten specimens had the following dimensions: 500 mm length (S), 200 mm width (b) and core thickness (t) of 80 mm .The facings' thickness (t) in specimens EC1 to EC5 was approximately 1 mm.

The edgewise compressive test was carried out using the universal testing machine along with the rest of the previously described data acquisition system.

In the edgewise compressive tests, the load was applied by two rectangular clamps (upper and lower) applied to the loaded ends of the tested specimens. In each test, the upper clamp was connected to the crosshead cylinder of the universal machine through a pinned steel connection. The lower clamp was connected to the universal machine's lower cylinder through a fixed connection. Fig. 4 shows the support system and the load application system used in the edgewise compressive tests. Fig. 5 shows the results for the force applied (F) and the corresponding value for the crosshead cylinder displacement (δ).

In general, the behaviour of the specimens with facings was linear elastic until failure, which occurred by buckling of the facing as a consequence of local debonding. Because the CA core surface was uneven, debonding started at different points along the specimens, which led to different collapse forces and post-collapse behaviours.

The edgewise compressive behaviour of the EC6–EC10 specimens was similar to that of specimens EC1–EC2, with two main differences: collapse force and mode. The collapse mode consisted of global buckling of the specimen under forces much lower than
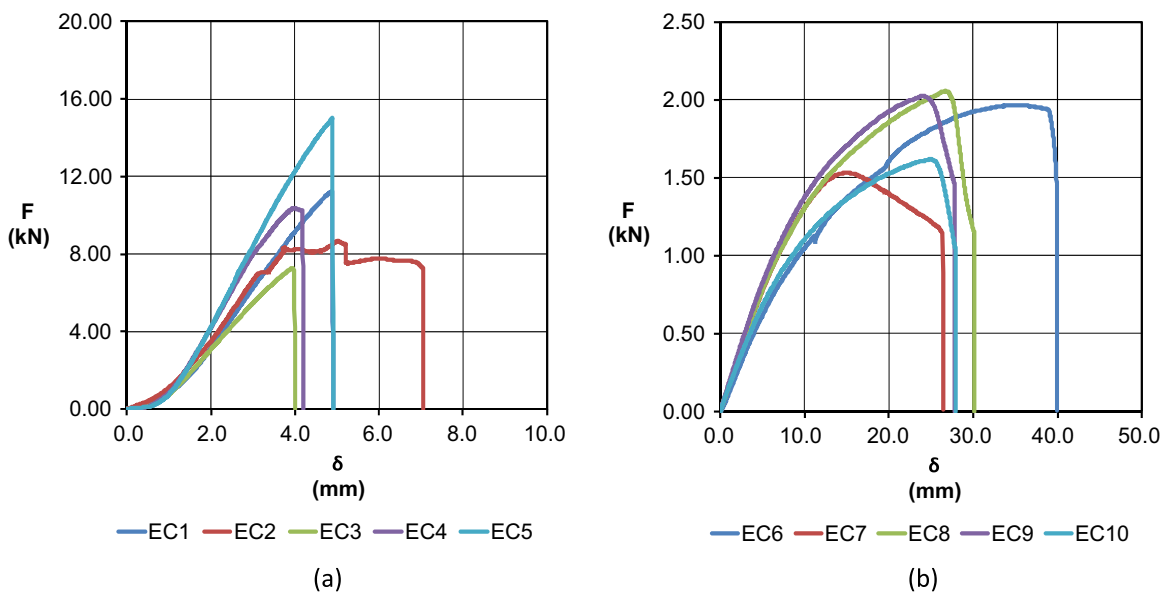

(a)

(b)

Fig. 5. Results of edgewise compressive tests on specimens EC1–EC5 (a) and specimens EC6–EC10 (b).
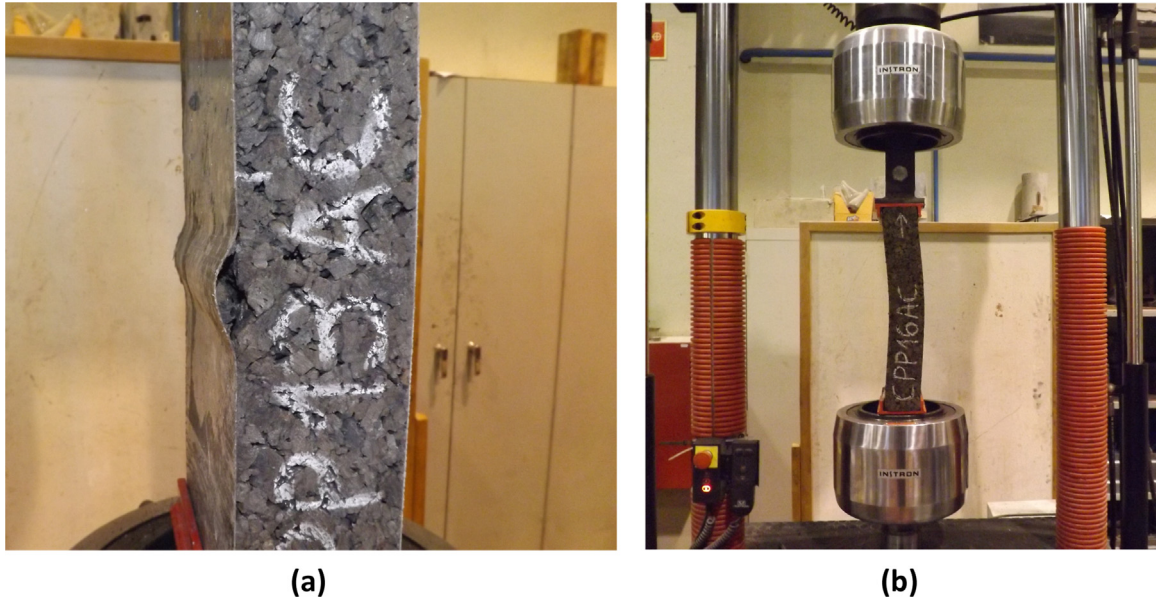
Fig. 6. Failure modes for test specimens during the edgewise compressive tests.

those of the specimens with facings.

The typical failure modes of specimens with and without facings subjected to edgewise compression are depicted in Fig. 6 (a) and (b), respectively.

According to [20], the edgewise compressive strength of the sandwich panel is given by expression (3)

$$\sigma_{ct}{}^{ult} = \frac{F_{max}}{A_t} \qquad (3)$$

Table 2 shows the results of the computed edgewise compressive resistance ($\sigma_{ct}{}^{ult}$) along with the values of F_{max} for each test specimen.

Although not mentioned in [20], the edgewise compressive Young's modulus (E_{ct}) for elastic behaviour was computed using the expression (4)

$$E_{ct} = \frac{\Delta\sigma}{\Delta\varepsilon} \qquad (4)$$

where:

1. E_{ct} – is the edgewise compressive modulus [MPa].
2. $\Delta\varepsilon$ – is the strain variation on the elastic slope of the stress–strain relationship [μmm/mm].
3. $\Delta\sigma$ – is the stress variation on the elastic slope of the stress–strain relationship [MPa].

Strain gauges were installed longitudinally in both facings of the EC1 and EC2 specimens to discriminate the contribution of the
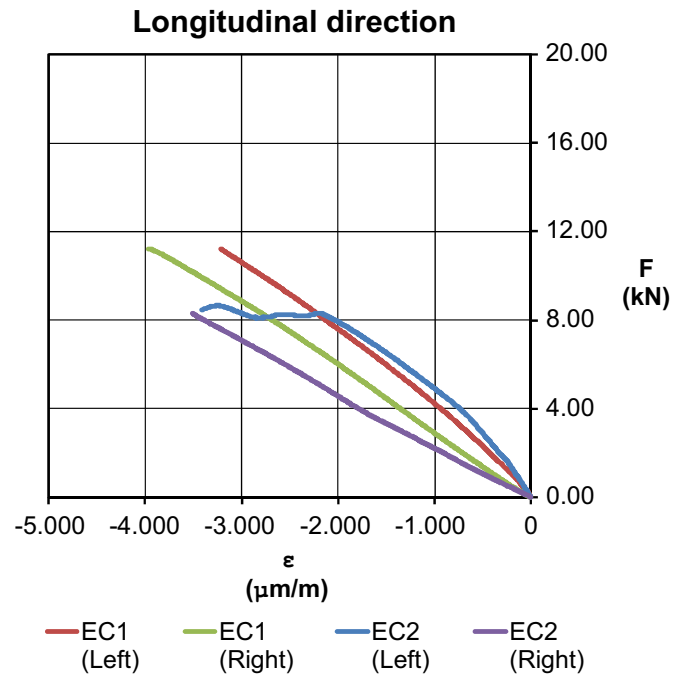

Fig. 7. Results for F–ε in edge wise compressive tests on EC1 and EC2.

GFRP facings to the edgewise compressive behaviour of the panels. Fig. 7 presents the measured strain versus total force for the instrumented tested specimens.

Given the results presented in Fig. 7, E_{ct} was computed considering the elastic slope defined by strains $\varepsilon_{1000} = |\varepsilon| = 1000$ μm/m and $\varepsilon_{2000} = |\varepsilon| = 2000$ μm/m. The F–ε results obtained from testing and the computed E_{ct} obtained from expression (4) are shown in Table 3. These results were considered as reference (E_{ct}) of specimens EC3, EC4 and EC5.

Since it was impossible to install strain gauges in the CA core due to its rather discontinuous surfaces, the elastic slope of the specimens without GFRP facings (EC6–EC10) was established between 0 kN $< F_{elast} <$ 1 kN and the corresponding values of (δ) (Fig. 5). The edgewise compressive modulus (E_{ct}) of specimens EC6 to EC10 was computed using expression (5)

Table 2
Results for the edgewise compressive strength of specimens EC1 to EC10.

	Specimen	F_{max} (kN)	A_t (mm²)	$\sigma_{ct}{}^{ult}$ (MPa)
With GFRP facings	EC1	11.23	502	22.37
	EC2	8.66	410	21.12
	EC3	7.28	385	18.90
	EC4	10.36	396	26.15
	EC5	15.01	420	35.73
Without GFRP facings	EC6	1.97	16000	0.12
	EC7	1.53	16000	0.10
	EC8	2.06	16008	0.13
	EC9	2.02	16000	0.13
	EC10	1.62	16000	0.10

Table 3
Edgewise compressive modulus (E_{ct}) of specimens EC1 and EC2.

Specimen	Facing	ε_{1000}			ε_{2000}			E_{ct} (GPa)
		ε (μm/m)	F_{1000} (kN)	σ_{1000} (MPa)	ε (μm/m)	F_{2000} (kN)	σ_{2000} (MPa)	
EC1	Upper	− 999.27	1.97	8.43	− 1999.66	3.540	15.12	**6.69**
	Lower	− 999.49	1.55	5.76	− 2001.23	3.213	11.98	**6.21**
EC2	Upper	− 999.60	2.46	11.97	− 1998.61	3.962	19.32	**7.35**
	Lower	− 999.37	1.11	5.41	− 2000.75	2.282	11.12	**5.71**

$$E_{ct} = \frac{\frac{\Delta F_{elast}}{A}}{\frac{\Delta \delta}{S}} \tag{5}$$

where

1. E_{ct} – is the edgewise compressive modulus [MPa].
2. ΔF_{elast} – is the load variation in the elastic slope considered [kN].
3. A – is the specimen cross section area [mm²].
4. $\Delta \delta$ - is the displacement elastic slope defined by ΔF_{elast} [mm].
5. S – is the distance between loading ends of specimen ($S = 500$ mm).

Table 4 summarises the results obtained for all the tested specimens regarding their edgewise compressive properties (σ_s^{ult}) and (E_{ct}).

The results show that the average value of σ_{ct}^{ult} for specimens without GFRP facings is only 0.5% of the σ_{ct}^{ult} for specimens with GFRP facings. In terms of edgewise compressive modulus E_{ct}, the average value of E_{ct} obtained for specimens without GFRP facings was found to be just 0.09% of the average value obtained for specimens with GFRP facings. As mentioned before, the failure mode was very similar for all specimens and occurred after local debonding and subsequent buckling of the GFRP facings. This means that the overall edgewise compressive behaviour of the composite solution is highly dependent on the combined behaviour of the compressive strength of the facings and core/facing bonding consistency. Given the observed edgewise compressive behaviour of this composite solution, it is possible to assume that the achieved value for the $\sigma_{ct}^{ult} = 24.85$ MPa could be used as reference for the average value of maximum compressive strength of the GFRP facings.

The results presented in Table 4 show some scatter of edgewise compressive properties which is attributed to the high variability of the intrinsic properties of the specimens' constituents, such as the GFRP cross section or the CA core stiffness. Also, the core/facing bonding consistency along the specimen might also influence this scatter. The results obtained in the flatwise and edgewise tests show values of σ_{ct}^{ult} similar to those given in [24].

Table 5 compares the results of the flatwise and edgewise

compressive tests. From these results it is possible to conclude that the flatwise deformation is essentially dependent on the CA core stiffness, since the variability of the compressive properties of specimens with and without GFRP facings is very low. On the other hand, the edgewise compressive tests show a significant difference between specimens with or without GFRP facings. It is quite clear from the results presented in Table 5 that the GFRP facings' compressive resistance and their bonding to the CA core play an important role in the edgewise compressive behaviour of these panels.

5. Beam flexure tests of composite specimens composed of cork agglomerate core and GFRP facings

These tests aimed to assess the flexure (bending) behaviour of composite panels composed of CA core and GFRP facings. The mechanical properties measured were the maximum bending moment (M_{max}), the maximum shear force (V_{max}), the ultimate shear stress (σ_{cs}^{ult}), the maximum axial tension on the GFRP facing (σ_f), the elasticity modulus of the GFRP facings (E_f), and the bending stiffness (D).

5.1. Tests for evaluation of the core shear properties by beam flexure

The determination of the core shear properties of panels with a CA core followed the test method described in [20]. For this purpose, a three point loading configuration (Fig. 8(a)) was considered, using the INSTRON 1343 loading equipment. It was adapted to guarantee a proper loading configuration. The knife shaped load (F) was applied at the mid-span of the specimen panel using a cylindrical steel bar coupled to the upper lift cylinder of the universal testing machine's crosshead (Fig. 8(b)).

According to [20], the loading equipment should be able to maintain a displacement speed around $v = 6$ mm/min. However, this speed was adjusted to $v = 4$ mm/min so that the maximum applied force (F_{max}) could be reached within 3–6 min of testing.

Five specimens were tested (CS1 to CS5), with the loading configuration depicted in Fig. 8(a). The span considered for the specimens' testing was $S = 435$ mm and the other dimensions

Table 4
Results for the edgewise properties of specimens EC1 to EC10.

	Specimens	F_{max} (kN)	δ (mm)	σ_{ct}^{ult} (MPa)	E_{ct}		Specimens	F_{max} (kN)	δ (mm)	σ_{ct}^{ult} (MPa)	E_{ct}
With GFRP facing	EC1	11.23	4.89	22.37	3.2 GPa	**Without GFRP facing**	EC6	1.97	34.74	0.12	3.4 MPa
	EC2	8.66	5.04	21.12	3.4 GPa		EC7	1.53	14.93	0.10	4.6 MPa
	EC3	7.28	3.94	18.90	3.4 GPa		EC8	2.06	26.69	0.13	4.6 MPa
	EC4	10.36	3.98	26.15	5.2 GPa		EC9	2.02	24.02	0.13	4.9 MPa
	EC5	15.01	4.89	35.73	4.9 GPa		EC10	1.62	24.99	0.10	3.67 MPa
	Average (X)	–	**4.55**	**24.85**	**4.55 GPa**		Average (X)	–	**25.07**	**0.11**	**4.2 MPa**
	Standard deviation (S_{n-1})	–	0.54	6.62	0.54		Standard deviation (S_{n-1})	–	7.07	0.02	0.67
	Coefficient of variation (CV)	–	11.86 %	26.65 %	11.86 %		Coefficient of variation (CV)	–	28.21 %	13.36 %	15.76 %

Table 5
Comparative study of the results of compressive properties obtained from flatwise and edgewise compressive tests.

Test	Panel	σ_{ct}^{ult} (MPa)	E_{ct}
Flatwise compression	**With GFRP facings**	61.47	3.07 MPa
	Without GFRP facings	60.88	3.04 MPa
Edgewise compression	**With GFRP facings**	24.85	4.03 GPa
	Without GFRP facings	0.11	4.23 MPa

were: length $L=500$ mm, width $b=200$ mm, total thickness (t) of approximately 82 mm (GFRP facings thickness of approximately 1 mm and CA thickness of approximately 80 mm). Using the aforementioned dimensions, shear of the CA core was expected to be the prevailing failure mode.

Fig. 9 depicts the force–displacement chart of the five tested sandwich specimens. As expected, the failure mode occurred by shear of the CA core of each of the tested specimens. Fig. 9 (b) shows the typical failure mode. The values of δ, also shown in Fig. 9(a), were obtained from the INSTRON displacement transducers and represent the relative displacement between the upper and lower hydraulic crossheads.

As shown in Fig. 9(a), all specimens had similar linear elastic behaviour followed by a brittle shear core failure. However, a more ductile behaviour was observed in specimens CS2 and CS5. This behaviour might be caused by the stronger influence of the facings on the specimens' behaviour, delaying core failure by shear and allowing some plastic deformations typical of bending-dominated behaviour. Nevertheless, the values of maximum force obtained for most of the specimens were very similar.

According to [21], the core shear ultimate stress is computed using expression (6):
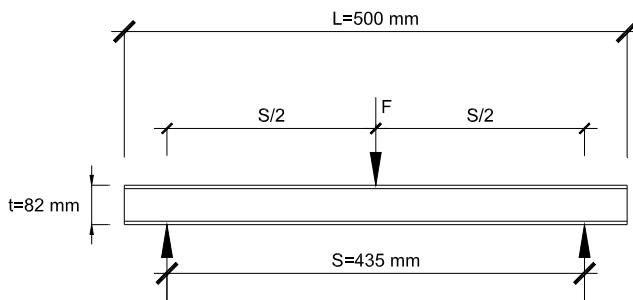
$$\sigma_{cs}^{ult} = \frac{F_{max}}{(d+c)b} \tag{6}$$

where:

1. σ_{cs}^{ult} – is the core ultimate shear stress [MPa].
2. F_{max} – is the maximum applied load [N.;
3. d – is the specimen total thickness [mm].
4. c – is the core thickness [mm].
5. b – is the specimen width [mm].

According to standard [20], the facings' axial stress (σ_f) is computed using expression (7):

$$\sigma_f = \frac{F_{max} \cdot S}{2t(d+c)b} \tag{7}$$

where

1. σ_f – is the stress in the GFRP facing [MPa].
2. F_{max} – is the maximum applied load [N].
3. c – is the core thickness [mm].
4. t – is the facing thickness [mm].
5. S – is the beam span [mm].

The values of maximum bending moment (M_{max}) and maximum shear force (V_{max}) were computed using the expressions $M_{max} = \frac{P_{max} \times S}{4}$ and $V_{max} = \frac{P_{max}}{2}$. Table 6 shows the results for the core shear properties.

Table 6 shows that the values of F_{max} applied to the specimens did not exceed 2 kN. Average core shear stress of the CA core ($\sigma_{cs}^{ult} = 53.66$ kPa) is compatible with the value of V_{max}, considering the relationship $V_{max} = \frac{P_{max}}{2}$ and the core section area for shear resistance. Thus, $\sigma_{cs}^{ult} = 53.66$ kPa could be taken as the average value of the core shear resistance for CA. Values obtained for the average axial stress of the facing obtained for GFRP facings ($\sigma_f = 12.52$ MPa) is only 50% of σ_f estimated after the edgewise tests.

However, since this test method is restricted to core or core-to-facing shear failure, the facing stress does not represent the ultimate strength σ_f of the facing. Hence, the computed average value $M_{max} = 0.95$ kN m/m also does not represent the average maximum moment of this composite solution.

In order to achieve relevant values for the maximum compressive stress σ_f, the flexural tests should be performed in such a manner that the applied moments produce significant curvature of the sandwich facing planes and result in compressive and tensile forces in the facings, thus inducing failure modes where the compressive behaviour of the GFRP facings is predominant.

The results presented in Table 6 show some scatter regarding the CA core shear properties. This scatter may result from the variability of the inherent properties of the tested specimens, such as the core thickness, the facing thickness or even the consistency of the bonding between the GFRP facings and the CA core.

The results obtained for the σ_{cs}^{ult} of CA core ($\sigma_{cs}^{ult} = 53.66$ kPa), when compared with results for other cores materials such as Rohacell or Nomex, indicate that σ_{cs}^{ult} of CA core corresponds to only 9% of the Rohacell maximum core stress of and 6% of the Nomex maximum [14].

5.2. Tests for evaluation of the composite beam flexural and shear stiffness (ASTM D7249/ASTM D7249M and ASTM D7250/D7250M)

The determination of the flexural properties and shear stiffness of panels with a CA core and GFRP facings followed the test method described in [21]. As in the previous flexural tests, a three point loading configuration was adopted, using the testing equipment INSTRON 1343 for controlled loading. Some adaptations had to be made to achieve the proper loading configuration.
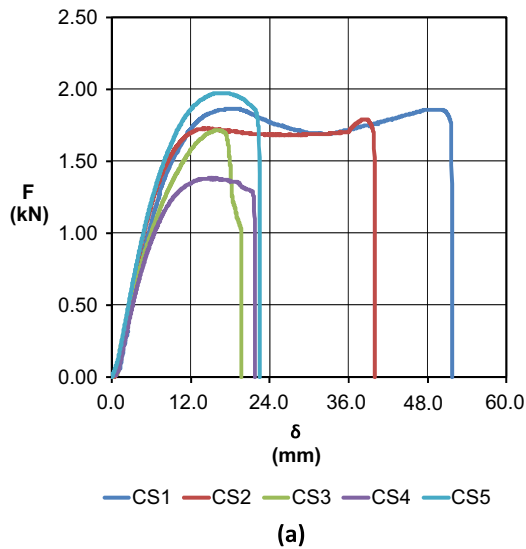

(a)   (b)

Fig. 8. Flexural tests: (a) 3 point loading configuration (based on [8]) and (b) setup for flexural tests.

Fig. 9. (a) Results from testing of specimens CS1–CS5 and (b) typical collapse mode in tests on specimens CS1–CS5.

Table 6
Results the tests for the evaluation of the core shear properties.

Test specimen	F_{max} (kN)	$\sigma_{cs}{}^{ult}$ (kPa)	σ_f (MPa)	V_{max} (kN/ m)	M_{max} (kN m/m)
CS1	1.87	57.34	13.16	4.66	1.01
CS2	1.79	54.93	13.08	4.48	0.97
CS3	1.72	52.74	12.37	4.29	0.93
CS4	1.38	42.40	10.24	3.46	0.75
CS5	1.98	60.91	13.73	4.94	1.07
Average ($\bar{X}$)	–	53.66	12.52	4.37	0.95
Standard deviation (S_{n-1})	–	6.99	1.36	0.56	0.12
Coefficient of variation (CV)	–	13.03 %	10.89 %	12.84 %	12.84 %

The knife shape load (F) was applied at mid-span of the panel specimen using a cylindrical steel bar coupled to the cylinder of the universal testing machine's crosshead.

According to [21], the loading equipment should maintain a loading speed of the order of $v=6$ mm/min and this speed should be adjusted so that the maximum applied force (F_{max}) is reached within 3 to 6 min of testing, leading, in these tests, to a speed of $v=4$ mm/min (Fig. 10).

A total of five specimens (F1–F5) were subjected to bending/shear tests. The testing setup involved applying an increasing mid-span load on simply supported beam specimens. The span considered for the specimens' testing was $S=935$ mm and the other dimensions were: length $L=1000$ mm, width $b=200$ mm, total thickness (t) of approximately 82 mm (GFRP facings thickness of approximately 1 mm and CA thickness of approximately 80 mm).

The testing equipment recorded the applied force (F) and the corresponding displacement δ. Fig. 11 shows the F–δ diagrams obtained from the tests performed on specimens F1–F5. Table 7 shows the values of F_{max} and its corresponding δ, as presented in Fig. 11.

As seen in Fig. 11, all the tested specimens showed essentially linear elastic behaviour before failure occurred through facing debonding, leading ultimately to buckling of the facing. However, elastic behaviour was observed for different associated values of F_{max}–δ. As expected, brittle failure occurred by facing buckling in all specimens.

Strain gauges were used on specimens F1 and F2 to record facing strains. The strain gauges were installed in the upper and lower facing of each specimen. The objective of this procedure was to determine the elasticity modulus of the GFRP facing E_f, as well as the flexural stiffness D.

Fig. 12(a) shows the force–strain (F–ε) relationship obtained from the bending tests performed on specimens F1 and F2. The strain gauge installed on the top facing of specimen F2 ceased functioning prematurely.

Flexural testing of specimens F1–F5 ended with the failure of each specimen. In most cases failure was the result of instability (buckling) of the upper facing (debonding from the CA core). Fig. 12(b) exemplifies this failure mechanism.

According to [21], the elastic modulus of GFRP facing (E_f) is computed using expression (8):
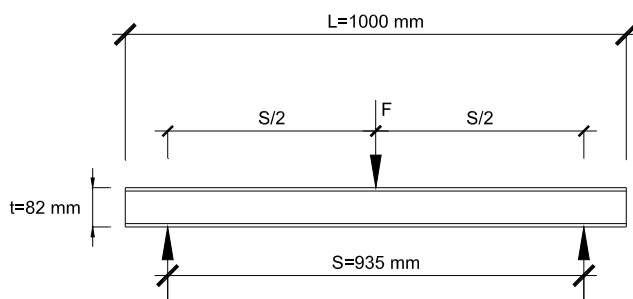

Fig. 10. Setup for the tests for evaluation of flexural and shear stiffness of specimens composed of CA core and GFRP facings.
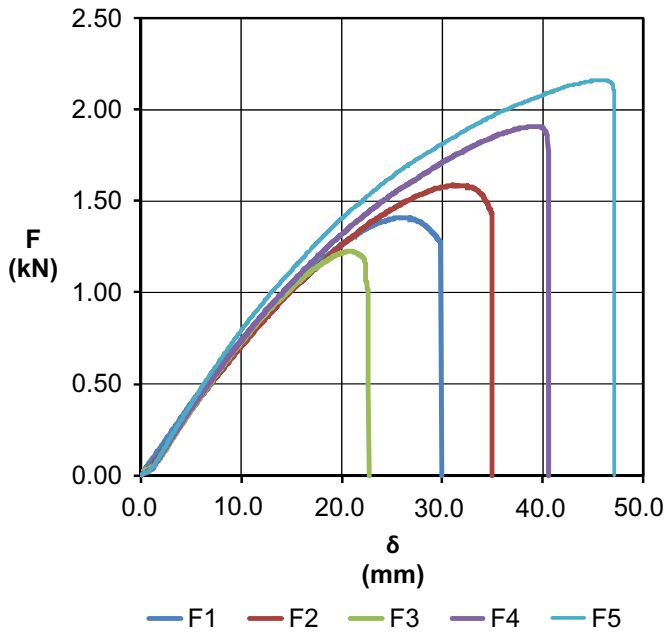
Fig. 11. $F–\delta$ diagrams obtained from the bending tests for specimens F1–F5.

Table 7
Results for $F–\delta$ relationship obtained for specimens F1 to F5.

Specimens	F_{max} (kN)	δ (mm)
F1	1.41	25.75
F2	1.59	31.08
F3	1.23	20.77
F4	1.91	39.40
F5	2.16	45.69

$$E_f = \frac{\sigma_{3000} - \sigma_{1000}}{\varepsilon_{3000} - \varepsilon_{1000}} \qquad (8)$$

Where:

1. E_f – elasticity modulus of GFRP facing [MPa].

2. ε_{1000} – strain result nearest to $\varepsilon = 1000$ µm/m.
3. ε_{3000} – strain result nearest to $\varepsilon = 3000$ µm/m.
4. σ_{1000} – associated stress value of ε_{1000} [µm/m].
5. σ_{3000} – associated stress value of ε_{3000} [µm/m].

According to the [21], the axial tension on the GFRP facing (σ_f) is computed using expression (9):

$$\sigma_f = \frac{F_{max} \cdot S}{2(d + c) b \cdot t} \qquad (9)$$

where

1. σ_f – is the facing axial tension [MPa].
2. F – is the maximum applied force [N].
3. S – is the specimen span [mm].
4. d – is the total thickness of the specimen [mm].
5. c – is the core thickness [mm].
6. b – is the specimen width [mm].
7. t – is the GFRP facing thickness [mm].

Table 8 shows the computed results for (E_f).

According to [21], in cases where shear flexibility is negligible, the effective sandwich flexural stiffness is computed using expression (10):

$$D^{7249} = \frac{S \times d}{4} \cdot \frac{F_{3000} - F_{1000}}{(\varepsilon_{\text{sup\_3000}} - \varepsilon_{\text{inf\_1000}}) + (\varepsilon_{\text{inf\_3000}} - \varepsilon_{\text{inf\_1000}})} \qquad (10)$$

where:

1. D^{7249} – is the effective flexural stiffness according to [22] [MPa].
2. S – is the total span [mm].
3. d – is the specimen total thickness [mm].
4. ε_{sup_1000} – is the top surface recorded strain value closest to $\varepsilon = 1000$ µm/m (top facing).
5. ε_{sup_3000} – is the top surface recorded strain value closest $\varepsilon = 3000$ µm/m (top facing).
6. F_{1000} – is the applied force corresponding to $\varepsilon_{sup-1000}$ [N].
7. F_{3000} – is the applied force corresponding to ε_{sup_3000} [N].
8. ε_{inf_1000} – is the bottom surface recorded strain value (magnitude) corresponding to F_{1000}.
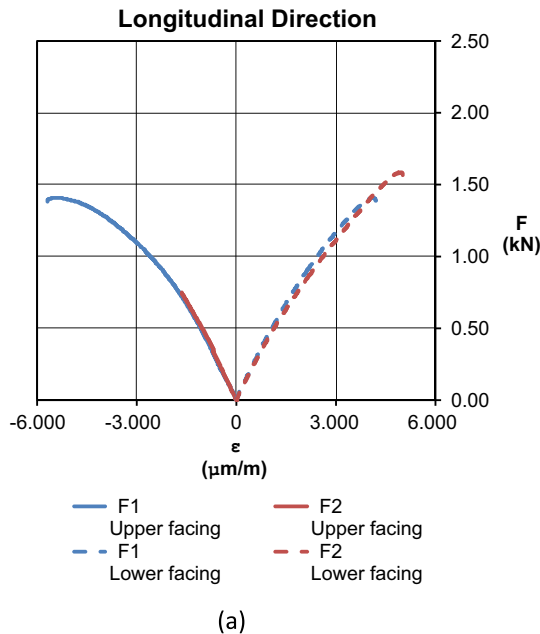

(a)

(b)

Fig. 12. (a) Stress–strain results for facings of specimens F1 and F2. (b) Failure mode of test specimens F1–F5.

Table 8
Results for computed elastic modulus of GFRP facings (E_f).

Specimen	Facing	t (mm)	ε_{1000}			ε_{3000}		
			ε (μm/m)	F_{1000} (kN)	σ_{1000} (MPa)	ε (μm/m)	F_{3000} (kN)	σ_{3000} (MPa)
F1	Upper	0.87	− 999.9	0.467	8.33	− 2997.6	1.096	19.53
	Lower	0.84	998.5	0.474	8.72	2998.4	1.168	21.51
F2	Upper	1.00	− 998.5	0.488	7.52	− 1645.6	0.750	11.55
	Lower	0.87	997.9	0.445	7.85	1498.5	0.631	11.14

9. ε_{inf_3000} – is the bottom surface recorded strain value (magnitude) corresponding to F_{3000}.

However, according to [22], in cases where shear flexibility is not negligible and the facings are identical, the flexural stiffness (D) is computed using expression (11).

$$D^{7250} = \frac{E_f \left(d^3 - c^3 \right) b}{12}$$

(11)

where

1. D^{7250} – is the effective flexural stiffness according to [22] [MPa].
2. E_f – is the elastic modulus of GFRP facing (assuming the average given in Table 9).
3. c – is the cork agglomerate CA core thickness$= d - 2t$, [mm].
4. t – is the GFRP facing thickness [mm].
5. d – is the specimen total thickness [mm].
6. b – is the specimen width [mm].

Table 9 summarises the results of the flexural tests conducted in accordance with [21] and [22], namely the flexural modulus D, the shear stiffness U and the shear modulus of the CA core G. Table 9 shows the results obtained as well as the statistical treatment of the results. In addition, Table 9 presents the computed values of elastic modulus Ef and the compression stress σf of the GFRP facings.

These results have a limited variation regarding E_f values, both for the values in tension E_f^t and in compression E_f^c. For the computation of D^{7250} values, the previously determined average value of E_f^c was used. However, the values obtained for D^{7249} and D^{7250} are quite similar given that the average value of D^{7250} is approximately 98.5 % of the average value of D^{7249}, which indicates that shear flexibility is negligible in the flexural behaviour of this composite solution.

Since failure of all specimens occurred by buckling of the GFRP facings, sufficient curvature was imposed in testing in order to estimate not only the M_{max} but also σ_f more accurately. Computed

Table 9
Results for the flexural properties of the tested specimens.

Specimen	E_f^C (GPa)	E_f^T (GPa)	σ_f (MPa)	M_{max} (kN m/m)	D^{D7249} (Pa m⁴)	D^{D7250} (Pa m⁴)
F1	5.61	6.40	20.35	1.76	3411	3837
F2	6.23	6.57	22.89	1.98	3914	4051
F3	–	–	17.71	1.53	–	4392
F4	–	–	27.53	2.38	–	4476
F5	–	–	31.18	2.70	–	4563
Average (X)	**5.92**	**6.48**	**23.93**	**2.07**	**3663**	**3606**
Standard deviation (S_{n-1})	0.44	0.12	5.4	0.5	355	259
Coefficient of variation (CV)	7.4%	1.9%	22.70%	22.70%	9.7%	7.2%

values for σ_f and M_{max} were, respectively, 23.93 MPa and 2.07 kNm/m (Table 9). These results are two times higher than the values presented in Table 6 for σf and M_{max}. Also, when comparing the results of the edgewise compressive tests and those of the flexural tests, we can see that the average value for σf of GFRP facings given in Table 9 corresponds to 96.3 % of σ_{ct}^{ult} (see Table 4). Given that edgewise compressive strength and flexural strength are both determined by the compressive behaviour of the GFRP facings, the average value for the maximum compressive stress in the GFRP facings of this composite solution should be limited to $\sigma_f^c = 23.93$ MPa.

Additionally, it should be noted that de elasticity modulus value obtained according to the [21] specifications ($E_f^c = 5.92$ GPa) is slightly higher than that obtained earlier in the edgewise compressive tests ($E_{ct} = 4.03$ GPa). Despite this difference, the influence of the facings is also quite clear in the flexural behaviour of these composite specimens.

6. Impact tests on panels composed of cork agglomerate core and GFRP facings.

The impact tests were carried out in accordance with [23] to assess the behaviour of panels when subjected to impacts from different bodies with different values of impact energy. In this particular case, the boundary conditions and overall dimensions of the panels were established so as to reproduce the real conditions for a wall panel assembly in buildings.

According to [23], the test method should simulate various types of impact, such as:

- Impacts of small rigid bodies; e.g. impact of stones hurled from the outside or the impact of furniture inside.
- Exceptional impacts from the interior; e.g. impacts of humans, animals or other deformable objects.
- Exceptional impacts from the outside; e.g. impacts resulting from humans or animals bumping against the wall.

The test specimens were subjected to impacts from pre-determined objects with different energy levels. The objective was to simulate impact in service and in ultimate state. Table 10 shows the different impact tests carried out as well as the compliance criteria for both service and ultimate state according to [23].

The test specimen's composition and dimensions were defined according to the project definition. Therefore, the core of the test specimen P1 was composed of two layers of 40 mm thick CA plates whereas the facings were composed of 1 mm thick GFRP sheets. The CA plates were overlapped to ensure the vertical misalignment of the joints. The specimen P1 had a total height (H) of 2250 mm and total width (b) of 1170 mm.

The setup for the impact tests (Fig. 14(b)) was assembled in a steel frame with a HEB 300 beam and two HEB 300 columns. The upper connection of the panels (Fig. 13(a)) was fixed using a cold formed profile beam (rigidly connected to the HEB 300 beam). The lower panel connection was also fixed using a cold formed profile

Table 10
Impact test for service limit state and ultimate limit state [11].

Service limit state for impact test compliance criteria: no penetration and no degradation				Ultimate limit state for impact test compliance criteria: no collapse, no penetration and no projection			
Test	Body of impact (kgf)	No. of impacts	Energy of impact (J)	Test	Body of impact (kgf)	No. impacts	Energy of impact (J)
1	0.5	3	1, 3 and 6*	3	1	1	10
2	50	3	100, 200 and 300**	4	50	1	700

* Energy values for the first, second and third impacts respectively.
** Energy values for the first, second and third impacts respectively.

beam (Fig. 13(b)), but this time the beam was rigidly connected to a 20 mm thick OSB plate. The OSB plate was fixed with 500 kgf concrete blocks on and along its back face. The pendulum setup to produce the impact of the bodies against the panel specimens was made using auxiliary cables and the laboratory's single girder bridge crane.

A steel cable system was added to this test setup to allow, along with the single girder bridge crane, the application of different types of impact and impact energies as indicated in [24]

The impact bodies used during the tests carried out on specimen P1 were as follows:

- 50 mm diameter, 0.50 kgf weight steel sphere,
- 62.5 mm diameter, 1 kgf weight steel sphere,
- 400 mm diameter, 50 kgf weight sphero-conical bag.

Regarding the sphero-conical 400 mm diameter bag, the weight of 50 kgf was obtained using 2.5 mm diameter glass beads as filling, as indicated in [24].

The energy E value of the impact bodies was determined according to expression (12):

$$E = p \times H \tag{12}$$

Where:

- E – is the impact energy [J],

- p – is the impact body weight [kgf],
- H – is the height measured between the designated point of impact and the height at which the impact body [m] is released (Fig. 14(a)).

According to [24], for the serviceability state, the expression of tests results consists of the following terms:

- No penetration: means that the test result is favourable because the impact body has not penetrated the facing of the test specimen on the impact side of the specimen.
- No degradation: means that the test result is favourable because after the test there are no visible (to the naked eye) cracks, depressions, protuberances or any other defects in the materials that could influence the fitness for use of the panel. Deformation, which only affects appearance, is acceptable but should be mentioned in the test report.

Regarding safety-in-use, the test results are expressed as follows:

- No collapse: means that the test result is favourable when, after the test, the panel retains its mechanical integrity and is still capable of sustaining its own weight in the test position.
- No penetration: means that the result is favourable because, after the test, the impact body has not passed through the test specimen.
- No projection: means that after the test, the impact body has not caused parts of the panel (e.g., core, facing, reinforcement, etc.) to project from the facing of the panel on the other side of the specimen from the impact side, creating sharp cutting edges or surfaces likely to cause personal injury by contact.

Since the standard used as reference for these tests does not prescribe any other specific damage assessment, the results were validated under the aforementioned terms by visual inspection.

Tables 11 and 12 present the impact body's characteristics, the impact parameters considered and the specimen behaviour when subjected to impact according to [23]. The results obtained through visual inspection of the validation criteria specified in [23] are also presented.

Since only one test specimen was used, the first tests performed were the serviceability state tests. After inducing the
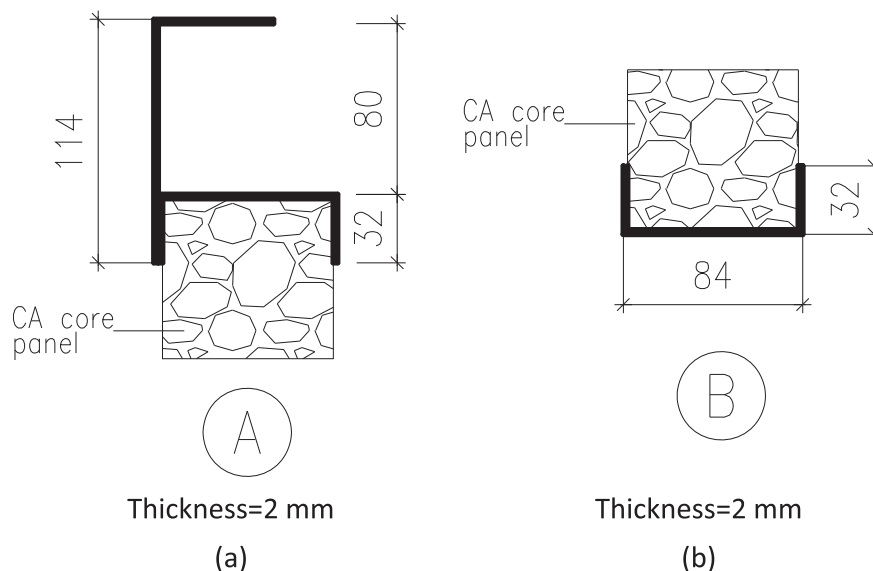

Thickness=2 mm

(a)

Thickness=2 mm

(b)

Fig. 13. Cold formed steel beam for the panels upper (a) and lower connection (b) (dimensions in mm).
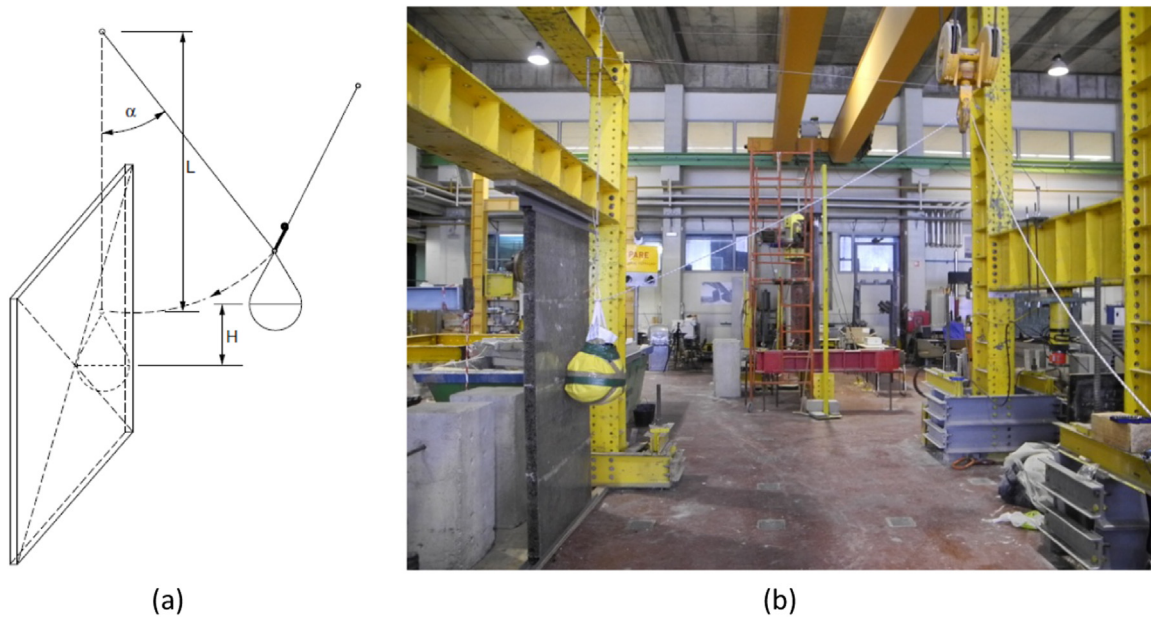
Fig. 14. (a) Impact on vertical assembly according to ISO 7892:2012 and (b) overall view of the vertical assembly for impact tests of P1 and P2 test specimens.

Table 11
Serviceability results for test specimen P1.

Serviceability results for test specimen P1					
Specimen	Test	Impact body (kgf)	h (m)	E (J)	Result
P1	1a	0.5	0.2	1	No penetration and no
P1	1b	0.5	0.6	3	degradation
P1	1c	0.5	1.2	6	
P1	2a	50	0.2	100	
P1	2b	50	0.4	200	
P1	2c	50	0.6	300	

Table 12
Safety-in-use results for test specimen P1.

Safety-in-use results for test specimen P1					
Specimen	Test	Impact body (kgf)	h (m)	E (J)	Result
P1	3a	1	1	10	No collapse, no penetration
P1	4a	50	1.4	700	and no projection

various impacts described in Table 11, none of the impact bodies penetrated the face of the test specimen on the impact side, and there were no visible defects in the materials and connections that could affect its fitness for use. Therefore, the panel under test was held to comply with the validation requirements and its safety-in-use was deemed satisfactory.

The safety-in-use tests were performed using the same P1 specimen. After the induced impacts described in Table 12., the specimen was shown to maintain its vertical integrity, since none of the impact bodies passed through the specimen or caused any significant damage to any of the facings. The specimen's upper and lower connections did not collapse and their deformation was not significant. Neither the elements nor parts of either the specimen or its connections suffered any kind of plastic deformation that could cause any personal injury by contact.

Fig. 15 shows the damage found in the test specimen after safety-in-use test.

Damage found in the test specimen, in particular the local

buckling of the facing, local crushing of the core material (Fig. 15 (b)) and the absence of core shear, could lead to the conclusion that impact behaviour of this wall panel is governed by bending. Hence, the compressive stress limit of facings and the crushing strength of the core material will be the parameters that govern the impact behaviour of sandwich panels to be used as wall assemblies in buildings. An important aspect of our work was the consideration of the actual connection profiles to be used in the panel assembly as a wall element. This procedure took into account the damping effect of the cold formed profile beams on the overall impact behaviour of the panel. Experimental and analytical studies of the specimen damping were not computed. Further experimental work on the impact behaviour of similar test specimens could surely provide some information about this matter. Nevertheless, the post-impact behaviour observed in specimen P1 indicates that both the panel and its connections show satisfactory behaviour to impact.

7. Fire resistance test on panels composed of cork agglomerate core and GFRP facings

The fire resistance of the composite panels was determined according to the test procedures described in EN 13501-2 [25]. This performance analysis refers only to the integrity (E) and thermal insulation (I) of panels composed of GFRP facings and CA core. Reaction to fire classification is not addressed in this paper.

Two panels were tested: one with no fire protection (P-CA) and another with a 12 mm thick fireproofing gypsum board (P-CA-FG). The dimensions of the specimens tested were 2280×1250 mm². The setup and procedure followed the specifications in [25], EN1363-1 [17] and EN1364-1 [26]. The resistance to fire classification is based on the exposure of the panels to a simulated fire scenario using the standard time–temperature curve, which corresponds to a fully developed fire inside a compartment [25]. This curve is given by expression (13):

$$T(t) = 345 \log_{10}(8t+1)+20 \qquad (13)$$

Where:

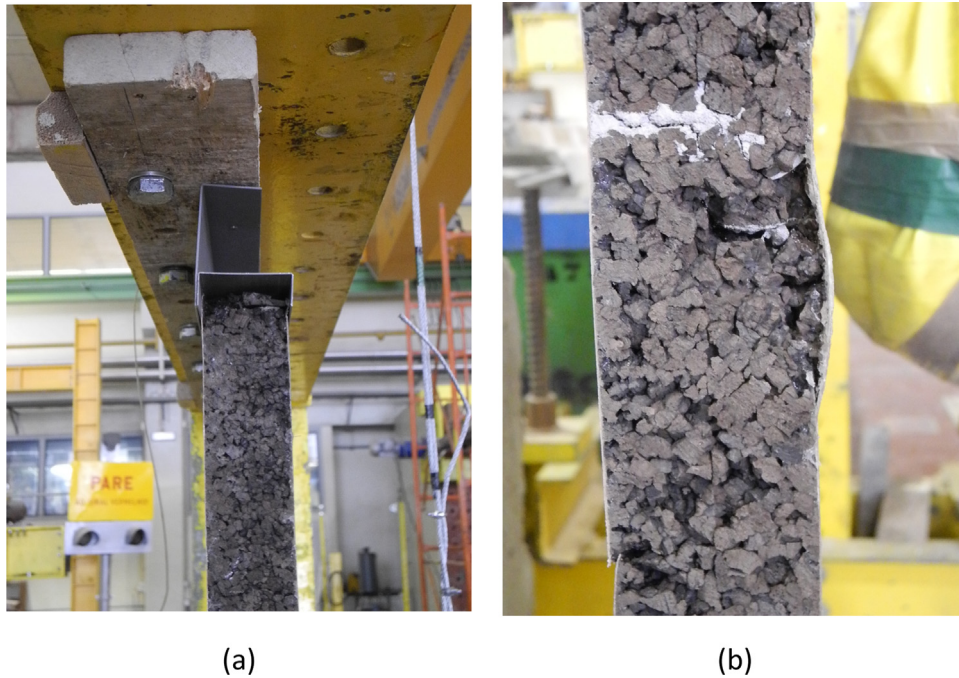1. t – is the time from the start of the test in minutes (min).

(a)   (b)

Fig. 15. Damage in specimen after safety-in-use impacts ((a) damage in upper connection and (b) damage in facing).

2. T – is the average temperature inside the furnace (°C).

The fire performance characteristics evaluated were the integrity (E) and thermal insulation (I) of composite wall assemblies consisting of CA core and GFRP facings. Integrity (E) refers to the ability of a construction element to withstand fire exposure on one side without transmitting flames or hot gases to the unexposed side. The assessment includes visual observation of significant cracking or sustained flaming on the unexposed side of the wall. Thermal insulation (I) refers to the ability of the construction element to withstand fire on one side without transmitting significant heat to the unexposed side. The assessment also includes recording the average temperature rise on the unexposed side to 140 °C above the initial temperature, with a maximum temperature rise of 180 °C. The designation of the fire resistance performance is a combination of the designation letters (E and I) and the elapsed exposure minutes of the nearest lower class in which the functional requirements are satisfied (EI15, 20, 30, 45, 60, 90, 120, 180 or 240) [25].

Temperatures on the wall assemblies were measured using type K thermocouples placed on the exposed surface (TE) and on the unexposed surface (TU), in both cases on the core/skin interface. In some test specimens, other type K thermocouples were placed on the interface between two layers of core materials (TC). All thermocouples were positioned in duplicate at approximately mid-height and mid-width of the wall assemblies and were connected to the data acquisition unit (sampling frequency of 300 reading/minute on all channels). Every temperature value presented is the average value of at least two thermocouples. [25]. In the fire resistance test of sandwich panel (P-CA) seven thermocouples were used (T1–T7), and for panel (P-CA-FG) twelve thermocouples (T1–T12) were used. Figs. 16 and 17 show the temperature evolution in each of the tested panels, as well as the thermocouple distribution.
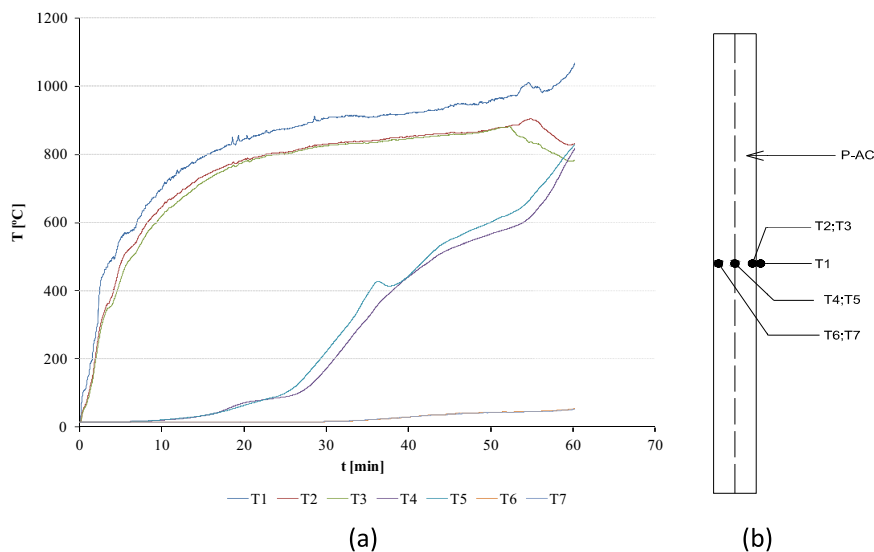

(a)   (b)

Fig. 16. Results for fire resistance test of panel P-CA. (a) Evolution of temperatures during the fire test and (b) distribution of the thermocouples in panel P-CA.
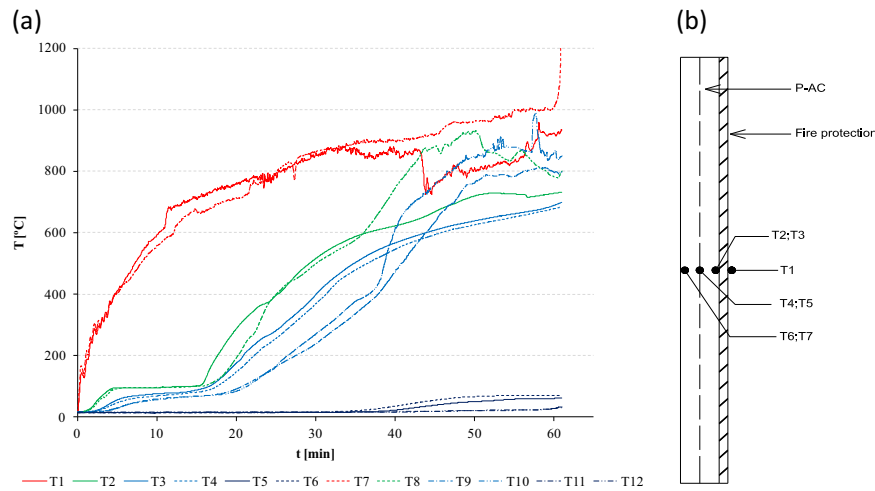
Fig. 17. Results for fire resistance test of panel P-CA-FG. (a) Evolution of temperatures during the fire test and (b) distribution of the thermocouples in panel P-CA-FG.

In this series of tests, the fire penetrated to the unexposed surface of the (P-CA) specimen after 55 min of exposure, although thermal analysis showed that the unexposed surface temperatures were well under the allowable limit. In this case, fire penetration occurred through the joints of the CA core plates. The fire protected wall assembly (P-CA-FG) lasted for a shorter time than the unprotected one. After careful examination, it was found that fire again breached through the joints of CA core plates. Both test specimens were classified as EI45 resistant. However, with proper care of these joints, EI60 classification can be achieved (Fig. 18).

The fire performance of test specimens (P-CA) and (P-CA-FG) was much more satisfactory than that observed in other solutions, such as sandwich wall panels with expanded polystyrene foam (EPS), which are classified from EI14 to EI30, depending on type of protection material used, or polyethylene terephthalate foam (PET) cores, classified as EI30 [27].

There could be several reasons for the improved fire performance of the CA core specimens relative to materials such as EPS or PET. The first could be that, given the very low percentage of hydrocarbons present in the cork agglomerate organic matrix, neither gases nor the materials in the cork agglomerates will fuel combustion during a fire and therefore the decomposition processes will tend to be slower. Another reason could be that during the degradation of the specimens, after the total decomposition of the GFRP facings, the CA core starts to directly experience the heat from the fire. At this point, the CA will tend to produce a fairly stable char formation, which will act as a natural protective layer and delay the heat flux to the external facing. In fact, the CA performs so well under fire exposure that placing fireproofing gypsum boards on the exposed surface has no significant impact on the fire resistance of the wall assembly.

8. Conclusions

This work set out to assess the mechanical (including impact) behaviour and fire resistance of a new configuration for sandwich
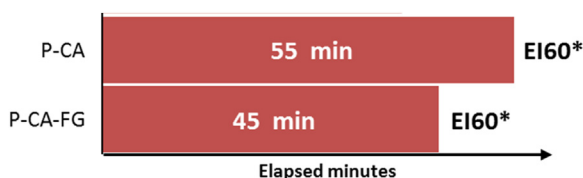

Fig. 18. Fire resistance classification of sandwich panels P-CA and P-CA-FG.

wall panels. These sandwich wall panels were composed of 88 mm thick core formed of cork agglomerate plates, and 1mm thick GFRP facings. The assessment was carried out through several experimental tests that complied with the recommendations of relevant standards.

The studies mentioned in chapter 2 provided relevant information about the different aspects of the development of this experimental work, i.e. the study of the mechanical, impact and fire resistance behaviour of sandwich panels. Moreover, some of the cited works provided relevant information about the behaviour of the materials currently used in composite solutions for wall panels and also provided important insight on the use and mechanical behaviour of cork agglomerate cores in composite solutions for purposes other than sandwich partition walls for buildings.

Regarding the flatwise compressive resistance of panels with GFRP facings and a CA core, experimental tests show that the GFRP facings' contribution to the flatwise compressive behaviour is negligible, given the small difference between the results obtained from specimens with and without such facings. However, these results yield rather small values of σ_{cn}^{ult} and E_{cn} for the CA core compared with other materials such as honeycomb polypropylene. In addition, with or without GFRP facings, the force–displacement relations derived from the tests showed the typical CA compressive behaviour.

The comparative study of the results of the flatwise and edgewise compressive tests showed that the flatwise deformation is essentially dependent on the CA core stiffness, since the variability of the compressive properties of specimens with and without GFRP facings is very slight. On the other hand, there is a significant difference between specimens with and without GFRP facings, which means that the GFRP facings' compressive resistance and their bonding to the CA core play an important role in the edgewise compressive behaviour of these panels. Further study and testing is needed to quantify this dependence and its relevance to edgewise compressive behaviour. However, the results showed that the σ_{cs}^{ult} of the CA core is quite small compared with other materials such as Rohacell® or Nomex®.

An important aspect of the impact behaviour assessment of these panels was the consideration in the experimental setup of the actual connection detailing to be used in the panel assembly as a wall element. This feature of the experimental setup made it possible to consider the additional damping provided by the cold formed profile beams in the overall impact behaviour of the panel. The behaviour observed during the impact tests on specimen P1 shows that the impact behaviour of the panel and its connections was satisfactory.

The fire resistance tests performed on panels with CA core and GFRP facings allowed the conclusion that the fire resistance of sandwich panels is closely related to the nature of the core material, especially to its thermal decomposition temperature and decomposition rate. As mentioned, the slow decomposition rate of the CA core is due to the charred layer, which slows the burning process and therefore improves the fire resistance of the wall assembly. In fact, cork agglomerate performs so well under fire exposure that installing fireproofing gypsum boards on the exposed surface does not have any significant effect on the fire resistance of the wall assembly. The fire performance of test specimens (P-CA) and (P-CA-FG) was much better than the performance of other solutions, such as sandwich wall panels with expanded polystyrene foam (EPS) or polyethylene terephthalate foam (PET) cores. Specimens of these were also tested but the details are not presented in this paper.

In conclusion, the proposed configuration of the CA core and GFRP facings for sandwich wall panels showed lower mechanical characteristics than other configurations using synthetic materials in their core. However, this alternative configuration was found to have substantially higher fire resistance than those using synthetic materials in their core. Thus, sandwich panels using CA core and GFRP facings could be a promising configuration for sandwich panel used for a non-structural wall. Additionally, as CA is a natural material, its usage as core for sandwich panels could be a step towards a more sustainable and eco-friendly solution for non structural wall construction systems.

Regarding the mechanical performance of sandwich panels using a CA core and GFRP facings, further study is needed to assess the enhancement of its mechanical properties.

Acknowledgements

References

[1] A. Zinno, A. Prota, E. Maio, C.E. Bakis, Experimental characterization of phenolic-impregnated honeycomb sandwich structures for transportation vehicles, J. Compos. Struct. 93 (2011) 2910–2924.
[2] S.S. Pendhari, T. Kant, Y.M. Desai, Application of polymer composites in civil construction: a general review, Compos. Struct. 84 (2008) 114–124.
[3] G. Zang, B. Wang, L. Ma, L. Wu, S. Pan, J. Yang, Energy absorbtion and low velocity impact response polyurethane foam filled pyramidal lattice core sandwich panels, J. Compos. Struct. 108 (2014) 304–310.
[4] M. Ei-Mikawi, A.S. Mosallam, A methodology for elevation of the use of advanced composites in structural civil enginnering applications, Compos. B Eng. 27 (1996) 203–215.
[5] J. Davies, Y.C. Wang, P.M. Wong, Polymer composites in fire, Compos. A Appl. Sci. Manuf 37 (2006) 1131–1141.
[6] G. Malucelli, F. Carosio, J. Alongi, A. Fina, A. Frache, G. Camino, Materials engineering for surface-confined flame retardancy, Mater. Sci. Eng. 84 (2014) 1–20.
[7] Y. Bai, T. Keller, J.R. Correia, F.A. Branco, J.G. Ferreira, Fire protection sysems for buildings floors made of pultruded GFRP profiles Part 2- modelling thermo-mechanical responses, Composites B 41 (2010) 630–636.
[8] Q.T. Nguyen, P. Tran, T.D. Ngo, P.A. Tran, P. Mendis, Experimental and computational investigations on fire resistance of GFRP composite for building façade, J. Compos. B 62 (2014) 218–229.
[9] N. Dodds, A.G. Gibson, D. Dewhurst, J. Davies, Fire behaviour of composite laminates, Compos. A Appl. Sci. Manuf. 31 (2000) 689–702.
[10] A.P. Mouritz, A.G. Gibson, Fire Properties of Polymer Composite Materials, Springer, Dordrecht, the Netherlands, 2006.
[11] S. Silva, et al., Cork : properties, capabilities and applications, Int. Mater. Rev. 50 (2005) 345–365.
[12] B. Soares, L. Reis, L. Sousa, Cork composites and their role in sustainable development, Procedia Eng. 10 (2011) 3214–3219.
[13] L. Smakosz, J. Tejchman, Evaluation of strength, deformability and failure mode of composite structural insulated panels, J. Mater. Des. 54 (2014) 1068–1082.
[14] O. Castro, J. Silva, T. Devezas, A. Silva, L. Gil, Cork agglomerates as an ideal material in lightweight structures, Mater. Des. 31 (2010) 425–432.
[15] R. Hoto, G. Furundarena, J.P. Torres, E. Munoz, J. Andrés, J.A. García, Flexural behaviour and water absorption of assymetrical sandwich composites from natural fibres and cork agglomerate core, Mater. Lett. 127 (2014) 48–52.
[16] INSTRON, "⟨⟨www.instron.us⟩⟩," 11 11 2014. [Online]. Available: ⟨⟨http://www.instron.us⟩⟩.
[17] EN 1363-1, Fire Resistance Tests - Part 1: General requirements, CEN, 1999.
[18] ASTM C365, Standard Test Method for Flatwise Compressive Properties of Sandwich Cores, ASTM, 2003.
[19] ASTM C364, Standard Test Method for Edgewise Compressive Strength of Sandwich Constructions, ASTM, 1999.
[20] ASTM C393/C393M, Standard Test Method for Core Shear Properties of Sandwich Constructions by Beam Flexure, 2006.
[21] ASTM D7249/D7249M, Standard Test Method for Facing Properties of Sandwich Constructions by Long Beam Flexure, 2006 .
[22] ASTM D7250/D7250M, Standard Practice for Determining Sandwich Beam Flexural and Shear Stiffness, ASTM, 2012.
[23] ISO 7892:, Vertical buildings elements - Impact resistance tests - Impact bodies and general test procedures, ISO, 2012.
[24] M. Mohamed, S. Anandan, Z. Huo, V. Birman, J. Volz, K. Chandrashenkhara, Manufacturing anda characterization of polyurethane based sandwich composite structures, Compos. Struct. 123 (2015) 169–179.
[25] EN 13501-2, Fire Classification of Construction Products and Building Elements, CEN, 2007.
[26] EN 1364-1, Fire Resistance Tests for Non-loadbearing Elements - Part 1: Walls, CEN, 1999.
[27] D. Pereira, T. Morgado, G. A, J. Proença, Fire performance of sandwich wall assemblies, IST (2014) (IST report).